

Atomistic modeling of large-scale metal film growth fronts

U. Hansen and P. Vogl

Physik-Department and Walter Schottky Institut, Technische Universität München, D-85748 Garching, Germany

V. Fiorentini

*Physik-Department and Walter Schottky Institut, Technische Universität München, D-85748 Garching, Germany
and Istituto Nazionale per la Fisica della Materia and Dipartimento di Fisica, Università di Cagliari, Cagliari, Italy*

(Received 21 September 1998)

We present simulations of metallization morphologies under ionized sputter-deposition conditions. By means of molecular-dynamics simulations using a carefully designed interaction potential, we analyze the surface adsorption, reflection, and etching reactions taking place during Al physical vapor deposition, and calculate their relative probabilities. These probabilities are then employed in a feature-scale cellular-automaton simulator, which produces calculated film morphologies in excellent agreement with scanning-electron-microscopy data on ionized sputter deposition. [S0163-1829(99)51612-3]

In this paper we present results of a hierarchy of theoretical models developed to describe the growth of metal thin films. Atomic-scale molecular dynamics (MD) and a feature-scale cellular-automaton simulator are combined to yield realistic simulations of film growth during physical vapor metallization of contact vias typical of semiconductor device technology. The MD simulations, accounting in full for the microscopic many-atom dynamics, are used to predict the reaction rates of the processes relevant in physical vapor deposition; the cellular-automaton simulator incorporates the reaction rates thus obtained, enabling us to predict and understand the topography of μm -scale film fronts, and their relationship to substrate geometry, incident beam energy, and angular beam distribution. Our approach yields a consistent and computationally efficient scheme to predict the topography of metal films on arbitrarily shaped substrates. A comparison with scanning-electron-microscopy (SEM) data on sputter-deposited Al-covered trenches demonstrates an excellent level of agreement between theory and experiment.

Our theoretical approach proceeds in three steps, namely (i) a classical interatomic interaction potential for Al is developed, (ii) reaction rates for Al atoms incident on Al surfaces are calculated therewith in a MD simulation, and (iii) a cellular automaton is developed and employed to simulate μm -scale film fronts, using the reaction rates extracted from MD. In the following, we analyze this procedure and present the relevant results for each step.

Interatomic potential. Previously developed classical interatomic potentials¹⁻⁷ for Al-Al interactions have mostly focused on bulk and molecular properties. The Ercolessi-Adams potential⁶ is a partial exception since, besides reproducing quantitatively the bulk and elastic properties of Al, it also yields interlayer relaxations⁶ in good agreement with experiment.⁸ Using this potential, we obtain surface energies in excellent agreement with *ab initio* calculations.⁹ We thus chose this model as a starting point to develop a new classical many-body potential for Al. Our own potential is carefully designed to reproduce the properties of Al aggregates in a wide range of bonding configurations (from bulk Al to Al surfaces and Al molecules), with special regard to

surface properties. Its functionalities significantly extend those of previous embedded atom models, while maintaining a high level of accuracy in reproducing Al bulk properties and surface formation energies.⁶ *First*, we introduced an exponential repulsive pair potential^{10,11} to account for the short-range interaction of Al atoms with kinetic energies exceeding 10 eV; this is a key requirement, as the kinetic energies of deposited atoms reach over 150 eV during ionized physical vapor deposition. *Second*, the embedding function has been readjusted to reproduce observed properties of low-density Al structures; after these changes, we obtained a significantly improved agreement of several reference quantities¹² in comparison to *ab initio* results^{13,14} and/or experiment.^{15,16} *Third*, we introduced a polynomial cutoff function, that smoothly terminates the interaction range of our potential at an interatomic distance slightly larger than the third-nearest-neighbor distance in bulk Al.

As a further test of our potential, we calculated the barriers for homodiffusion on the low-index faces of fcc Al. Specifically, we considered hopping on Al(110) along and orthogonal to the $[1\bar{1}0]$ -oriented rows, hopping on Al(100), and concerted exchange on Al(100). The general level of agreement with *ab initio* density-functional calculations^{13,14} is very good (as can be seen in Table I), giving us further confidence in the accuracy of our potential.

Reaction rates from molecular dynamics. In the second step of our approach, reaction probabilities were calculated in classical molecular-dynamics simulations using our Al interaction potential. In particular we determined, as a function of the energy and off-normal angle of incident Al atoms, the probability of three processes: adsorption, reflection, and etching (in the latter, the incoming atom's impact on the surface causes the kick-out of one or more substrate atoms). Supercells containing 1320 atoms arranged in 10 atomic layers are employed; cell dimensions are chosen so as to avoid artifacts of the in-plane periodicity. The starting configuration is chosen to be a (111) surface, the one Al surface with the lowest formation energy. All atomic coordinates are allowed to evolve dynamically, except those of the two bottom

TABLE I. Comparison of selected hopping and exchange diffusion barriers on low-index Al surfaces obtained with the present model and in *ab initio* calculations. Al (111) is also included for completeness.

	This work	<i>Ab initio</i>
Al (111) hopping	0.04	0.04 ^a
Al (100) hopping	0.60	0.68, ^a 0.65 ^b
Al (100) exchange	0.50	0.35 ^a
Al (110) \perp hopping	1.13	1.06 ^a
Al (110) \parallel hopping	0.30	0.60 ^a

^aReference 13.

^bReference 14.

layers of the supercell. The surface temperature is set at 450 K (i.e., about 1/2 of the melting temperature, and 20% larger than the bulk Debye temperature).

We start our simulations with the incident Al atom placed outside the interaction range of the surface. Its initial kinetic energy is set in the range of 25 to 125 eV, and its starting angle off the surface normal in the range 0° to 60° , which corresponds to typical ionized physical vapor deposition conditions. Due to the assumption of validity of the Born-Oppenheimer approximation implicit in classical molecular-dynamics simulations, intra-atomic electronic excitation effects are not accounted for in our calculations. This is justified since typical relaxation times for electronic excitations are much shorter than the timescale of interest in our study, and also because the energies involved are much smaller. The trajectories of the incident atom, and of any other atom which may be etched away from the surface upon impact, are then monitored until either a certain time span has elapsed, or the outgoing atoms (in the case of reflection or etching) have traveled a distance of 10 \AA away from the surface. Analyzing 200 trajectories per incident energy and angle, we collected a statistically significant sample of well-defined adsorption, reflection, and etching events. The relative probability of the corresponding process is calculated as the ratio of the number of events of each kind to the total number. The typical statistical error in the reaction probabilities thus determined is below 5%.

The behavior of reflection, adsorption, and etch rates as a function of off-normal angle are summarized in Fig. 1 for two representative incident kinetic energies, namely 25 eV in panel (a), and 100 eV in panel (b). At low energies [panel (a)] the adsorption probability (thick solid line, squares) decreases from near unity for angles below 20° to approximately 1/2 for angles in the range of 60° . This decrease is compensated by a corresponding increase in the reflection probability (dashed line, triangles). At low energy, etch processes (thin solid line, circles) are negligible at all angles. Increasing the incident kinetic energy to 100 eV, we find considerable changes in the relative reaction probabilities. Even at small angles, the reflection probability is nonvanishing; the adsorption probability is correspondingly reduced, and is now below 0.7 at all angles. More interestingly, the etching probability is always nonzero, it reaches a maximum of 0.4 at 50° , then decreases as near-grazing angles are approached. For small deviations from normal incidence, the etch rate initially raises, since the probability of a surface

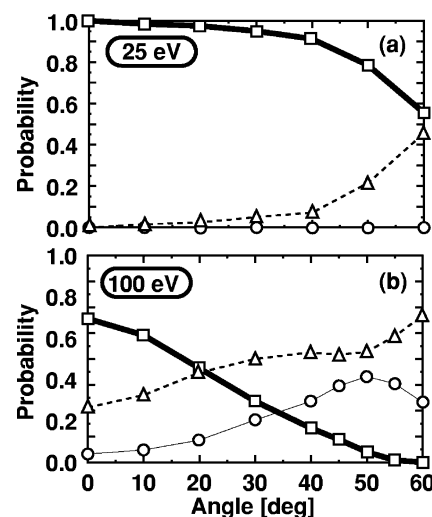


FIG. 1. Reaction probabilities for Al atoms impinging on Al(111) with a kinetic energy of 25 eV [panel (a)] and 100 eV [panel (b)] as a function of the off-normal angle. The processes considered are adsorption (thick solid line, squares), reflection (dashed line, triangles), and etching (thin solid line, circles).

atom to gain momentum directed away from the surface increases when the incoming atom arrives at an oblique angle at the surface. At large angles of incidence the etch rate drops because of the competing specular reflection events.

By adjusting the bias voltage between sputter source and deposition target during ionized physical vapor deposition, both the energy regimes just discussed are experimentally accessible. It is expected that they lead to rather different trench topographies, which we simulate with a cellular-automaton technique.

Feature-scale cellular-automaton simulator. In the final step of our approach, we have developed a two-dimensional cellular automaton to model the growing film front on a μm scale. The automaton accounts for the effects of flux shadowing, adsorption, reflection, etching, and surface diffusion. The simulated structure is represented in cross section by a two-dimensional grid. Each grid cell represents an Al atom, and is assumed to have a physical length of 2.5 \AA (the effective atomic diameter in Al bulk): thus, for example, a $1\text{-}\mu\text{m}$ -wide structure will be described by 4000 grid cells across.

The atoms are serially and independently emitted from the sputter source far above the surface according to a predetermined angular and energetic distribution, and move on a straight trajectory, determined also by the applied source-target bias, until they strike the growing film front. Interactions in the gas phase are neglected in view of the the low pressure (typically a few tenths of mTorr) and the resulting long mean free path typical of sputter deposition. Spontaneous desorption is also negligible in all the conditions considered.

The impact angle and energy of the atoms hitting the surface determine which process is activated upon impact.¹⁷ This may be any one of the three (adsorption, reflection, etching) whose rates have been previously calculated via MD simulations. If the atoms are reflected, or an etch process takes place, the path of the corresponding atoms is further traced until they hit the film surface for a second time. The three basic processes can then take place again, and so forth.

Finally, the atoms get either adsorbed, or escape back into the gas phase.

Adsorption presents some additional complications. The local diffusion and accommodation mechanism upon adsorption is a key ingredient in deposition models. A reasonable assumption is that incoming atoms are accommodated at a (local) minimum-energy site within one diffusion length from the landing site, the diffusion length being determined by the surface temperature and morphology, and the deposition rate. In the cases of interest here, the problem of determining an effective diffusion length for the adsorbed atoms is quite formidable for several reasons. On the one hand, one expects low effective diffusivity due to the very high experimental growth rate [not well controlled, but in the order of $0.5 \mu\text{m}/\text{min}$, or roughly $40 \text{ ML}/\text{sec}$ (Refs. 18 and 19)], and also because the growing surface rapidly loses its low-index character becoming essentially disordered. On the other hand, collision energies are large, and (although energy transfer mechanisms on rough surfaces are largely unknown) one may expect multiatom events and transient mobility effects to increase the effective diffusivity. We aim at using parameters that maximize the coordination of the new particle, with the constraint that the impact-to-final site distance is minimized (so that the local film curvature is minimized²⁰).

In practice, we set the following criteria for (i) the maximum diffusion distance, and (ii) the nature of a minimum-energy site:

(i) The *maximum* diffusion distance is taken to be $d_{\text{max}} = d_{\text{max}}^{\text{thr}} = 5 \text{ grid spacings} = 12 \text{ \AA}$. All sites within this distance from the landing site are analyzed; the chosen final site is the one *closest* to the landing site, among those with the highest local coordination [to be defined below, point (ii)]. Because of this, the effective diffusion length is actually rather smaller than the maximum value d_{max} . Our specific choice of d_{max} may simply be regarded as a calibration factor designed to avoid dendritic structures or very flat surfaces which are not observed in the experimental regime of interest here. However, we find a rather sharp change in the dependence of the surface roughness on d_{max} , from rather weak for $d_{\text{max}} > d_{\text{max}}^{\text{thr}}$ to strong for $d_{\text{max}} < d_{\text{max}}^{\text{thr}}$.²¹ Thus our value $d_{\text{max}}^{\text{thr}}$ is effectively a crossover threshold between the two regimes mentioned. In effect, the SEM micrographs show sharp cusps in the rooflike structures suggesting that no long-range diffusion occurs in experiment. This seems to make sense given the extremely high deposition rate, and the roughness of the growing surface.

(ii) A minimum-energy site is defined in terms of its local coordination²² as follows: for each candidate site within the preset maximum distance from the landing site [point (i)] we calculate the number of atoms contained in a circle centered at the candidate site and with a radius of 7 grid spacings. This criterion amounts to selecting the site with maximum *average* coordination; while similar to that of highest first-neighbor coordination, contrary to the latter it avoids pathological choices such as high coordination sites on highly ramified structures.

Results of topography simulations. Figure 2 depicts trench topographies predicted by our model for different deposition conditions, compared to scanning-electron-microscope pictures taken in similar conditions.¹⁸ The structure size is 1.2

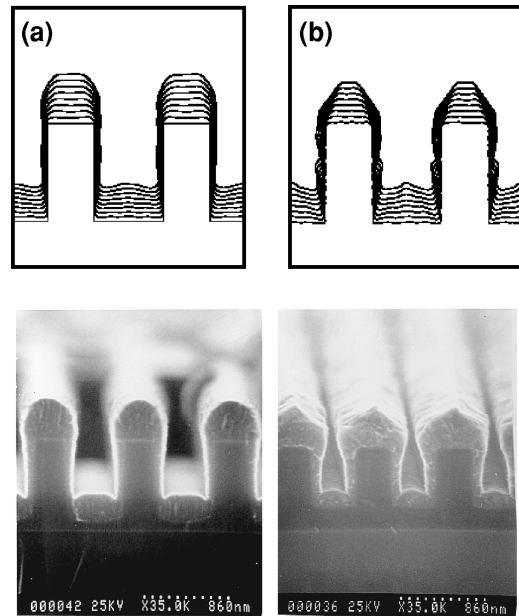


FIG. 2. Film morphologies on trench structures predicted for different ionized magnetron sputtering conditions compared to experiments (Ref. 18). In panel (a) we set 80% ionization, and 10 V bias, in panel (b) 80% ionization, and 80 V bias. The material we deposited in (a) and (b) corresponds to a total number of 16×10^6 atoms. Below, a SEM micrograph with experimental results.

μm across. In the cellular-automaton simulation, the emitted atom energies are picked from a Thompson distribution centered at 3 eV, as suggested experimentally.^{19,23} The initial angles of the nonionized atoms are chosen from a collimated cosine distribution with a maximum off-normal angle of 40° . To mimic the experimental conditions, we assume that 80% of the emitted Al atoms get onefold ionized; for these atoms, the trajectory and impact energy change according to the applied source-target bias.

We now describe our results for different values of the the sputter source-to-target bias corresponding to the low and high energy regimes identified in our MD calculations. The results in panel (a) of Fig. 2 were obtained setting the bias to 10 eV. In agreement with experiment (also displayed in Fig. 2), we predict a film growth front of rounded shape on top of the feature and, due to geometric shadowing, a reduced film thickness at the bottom of the trench. The pile-up at the center of the trench is not only of geometric origin, but also partly due to reflections of atoms impinging on the trench sidewalls. In panel (b) of Fig. 2 we report results obtained with a bias of 80 eV. Our calculations predict, in accord with experiment, a rooflike structure on top of the feature. This structure is due to the preferential etching at angles of 50° [see Fig. 1(a)] which leads to a lower deposition rate on the rooflike structure. Simulations of structures scaled down in size by a similarity transformation,²⁴ (i.e., with the same geometry, relative sizes, and aspect ratios) produced very close results, suggesting that the profiles obtained are largely self-similar at these length scales.²⁴

In conclusion, we have demonstrated the viability of accurate simulations of mesoscopic thin film morphology based on atomic-scale simulations. We performed detailed theoretical calculations of the probabilities for surface reactions taking place during ionized physical vapor deposition

conditions, and combined these predictions with μm -scale cellular-automaton simulations. Our molecular-dynamics calculations revealed strongly energy-dependent adsorption, reflection, and etch rates (the latter exhibiting a distinct maximum for high incident kinetic energies at $\sim 50^\circ$). We were able to predict topographies of metal films deposited on trench structures under different ionized physical vapor deposition conditions in remarkable agreement with experiment. Our results represent a major step ahead over earlier

thin film growth models based on rate equations,²⁵ which did not incorporate beam-energy-dependent surface reactions on an atomistic scale.

We gratefully acknowledge financial support by Siemens AG. We thank Dr. A. Kersch and Dr. A. Spitzer for valuable guidance throughout the project, Dr. P. Ruggerone for a critical reading, and Dr. F. Ercolessi for helpful assistance. V.F. was supported by the Alexander von Humboldt-Stiftung during his stay at the Walter Schottky Institut.

- ¹M. S. Daw and M. I. Baskes, Phys. Rev. Lett. **50**, 1285 (1983); Phys. Rev. B **29**, 6443 (1984).
- ²J. Cai and Y. Y. Ye, Phys. Rev. B **54**, 8398 (1996).
- ³R. G. Hoagland, M. S. Daw, S. M. Foiles, and M. I. Baskes, J. Mater. Res. **5**, 313 (1990).
- ⁴M. I. Baskes, Phys. Rev. B **46**, 2727 (1992).
- ⁵J. Mei and J. W. Davenport, Phys. Rev. B **46**, 21 (1992).
- ⁶F. Ercolessi and J. B. Adams, Europhys. Lett. **26**, 583 (1994).
- ⁷A. F. Voter and S. P. Chen, in *Characterization of Defects in Materials*, edited by R. W. Siegel, J. R. Weertman, and R. Sinclair, MRS Symposia Proceedings No. 82 (Materials Research Society, Pittsburgh, 1987), p. 175.
- ⁸G. N. Kamm and G. A. Alers, J. Appl. Phys. **35**, 327 (1964).
- ⁹V. B. Deyirmenjian, V. Heine, M. C. Payne, V. Milman, R. M. Lynden-Bell, and M. W. Finnis, Phys. Rev. B **52**, 15 191 (1995).
- ¹⁰A. A. Abrahamson, Phys. Rev. **178**, 178 (1969).
- ¹¹This potential is $V(r) = A \exp(-Br) - C$, with $A = 7255.44 \text{ eV}$, $B = 4.42085 \text{ \AA}^{-1}$, and $C = 1.04897 \text{ eV}$.
- ¹²The binding energy and vibrational energy of Al_2 , the (111) homodiffusion barrier, the adsorption energy per atom on Al (111), and the binding energy of Al_2 on Al (111) with respect to isolated adatoms are -1.4 eV , 290 cm^{-1} , 0.04 eV , 2.42 eV , and 0.50 eV . They compare very well with the reference values (all *ab initio* values from Ref. 13 unless otherwise specified) -1.4 eV ($-1.36 \pm 0.06 \text{ eV}$ experimental, Ref. 16), 284 cm^{-1} (experimental, Ref. 15), 0.04 eV , 3.06 eV , and 0.58 eV . The local-density approximation (LDA) adsorption energy is larger than ours due to the known LDA overbinding, but the two values agree well when expressed in percentage of the bulk binding energy ($\sim 73\%$).
- ¹³R. Stumpf and M. Scheffler, Phys. Rev. Lett. **72**, 254 (1994); Surf. Sci. **307**, 501 (1994); Phys. Rev. B **53**, 4958 (1996).
- ¹⁴P. J. Feibelman, Phys. Rev. Lett. **65**, 729 (1990).
- ¹⁵M. F. Cai, T. P. Djugan, and V. E. Bondybey, Chem. Phys. Lett. **155**, 430 (1989).
- ¹⁶Z. Fu, G. W. Lemire, G. A. Bishea and M. D. Morse, J. Chem. Phys. **93**, 8420 (1990).
- ¹⁷The local normal at the impact site is defined as the direction connecting the impact point to the center of mass of the atoms contained in a circle centered on the impact point and with radius of 10 grid spacings.
- ¹⁸S. Hamaguchi and S. M. Rossnagel, J. Vac. Sci. Technol. B **13**, 183 (1995).
- ¹⁹W. D. Westwood, in *Microelectronic Materials and Processes*, edited by R. A. Levy (Kluwer, Dordrecht, 1989), p. 133.
- ²⁰S. K. Dew, T. Smy, and M. J. Brett, IEEE Trans. Electron Devices **39**, 1599 (1992).
- ²¹This is due in part to the intrinsic asymmetry produced by the choice of the *closest* highest-coordination site among those within the d_{max} circle.
- ²²It is known [see, e.g., M. Methfessel, D. Hennig, and M. Scheffler, Appl. Phys. A: Solids Surf. **55**, 442 (1995), and references therein] that the binding energy of metals in a structure with local coordination C is given semiquantitatively by $E_{\text{bind}} = AC + B\sqrt{C}$, with A and B constants.
- ²³E. Dullini, Nucl. Instrum. Methods Phys. Res. B **2**, 610 (1984).
- ²⁴A. Barabasi and H. E. Stanley, *Fractal Concepts in Surface Growth* (Cambridge UP, Cambridge, England, 1995).
- ²⁵L. J. Friedrich, S. K. Dew, M. Brett, and T. Smy, Thin Solid Films **226**, 83 (1995); S. S. Winterton, T. Smy, S. K. Dew, and M. J. Brett, J. Appl. Phys. **78**, 3572 (1995); L. J. Friedrich, D. S. Gardner, S. K. Dew, M. J. Brett, and T. Smy, J. Vac. Sci. Technol. B **15**, 1780 (1997).